NACA RM E55D07b

NACA

RESEARCH MEMORANDUM

EXPLORATORY INVESTIGATION OF FLOW IN THE SEPARATED REGION AHEAD OF TWO BLUNT BODIES AT MACH NUMBER 2

By Harry Bernstein and William E. Brunk

Lewis Flight Propulsion Laboratory
Cleveland, Ohio

NATIONAL ADVISORY COMMITTEE
FOR AERONAUTICS

WASHINGTON

June 30, 1955
Declassified May 2, 1958

NACA RM E55D07b

NATIONAL ADVISORY COMMITTEE FOR AERONAUTICS

RESEARCH MEMORANDUM

EXPLORATORY INVESTIGATION OF FLOW IN THE SEPARATED REGION AHEAD OF TWO BLUNT BODIES AT MACH NUMBER 2

By Harry Bernstein and William E. Brunk

SUMMARY

Flow separation from a flat plate ahead of two blunt two-dimensional bodies was investigated in detail at Mach number 2.0. Interferograms were obtained for the separated regions, and the pitot-pressure distribution and flow directions were surveyed in one of the regions. Mach numbers calculated from density and pitot-pressure data were generally less than 0.5 in the reverse-flow regions near the plate surface. A flow-direction survey for a model with separation at the leading edge of the flat plate showed a reverse-flow component in about half the separated region. Static pressures along the plate surface and over the blunt body were sensitive to small disturbances and small changes in stream conditions.

INTRODUCTION

The separation of boundary layers ahead of blunt bodies in a supersonic stream has been studied and described by many investigators in recent years. Some qualitative results of these studies for turbulent boundary layers are as follows.

For two-dimensional bodies on a flat plate, the nature of the separation depends largely on the size of the body relative to the upstream boundary layer. For bodies of the same order of thickness as the boundary layer ("first regime")(ref. 1), the shock-boundary-layer interaction region covers a large portion of the separated flow, and the pressure distribution in the separated region varies considerably with body size. Pressures upstream of the separation point, however, appear to be independent of the cause of separation.

When the body is three or more times as thick as the boundary layer ("second regime"), the shock-boundary-layer interaction region is smaller in extent relative to the separated region, and a nearly constant pressure equal to that behind the separation-produced shock exists on a

large portion of the flat plate in the separated region. On the face of the blunt body, however, pressures can still vary considerably and depend on the shape of the body. The effective wedge angle corresponding to the constant-pressure portion of the separated region is nearly 13° for Mach numbers from about 2.0 to 4.0 (ref. 2).

As the body thickness is increased, the separation point moves upstream. For body thicknesses greater than about 15 percent of the upstream plate length, the separation point is close to or at the plate leading edge ("third regime"). If no roughness is used near the leading edge, the separation point moves into a region of laminar flow as it approaches the leading edge. Since the laminar layer cannot support as large a pressure change as the turbulent layer, the separation angle is reduced and the separation point moves rapidly to the leading edge.

If the body thickness is further increased (or the plate retracted), the angle of a line from the leading edge tangent to the body approaches the shock detachment angle corresponding to the free-stream Mach number. In this regime, unsteady flow is encountered if the blunt body has sharp edges. If the body is cylindrical, however, no oscillations are encountered, and a steady transition to the modified detached-shock-wave regime is observed. The oscillating flow (described in detail in refs. 3 and 4) may therefore be associated with the presence of sharp edges in the subsonic circulatory motion ahead of the body.

Although the preceding description applies specifically to two-dimensional bodies, the results are very similar for blunt axially symmetric bodies with projecting spikes or probes. In the latter case, however, the first regime, in which the body is of the same order of thickness as the boundary layer, is not easily produced and has not been studied.

This summary of previous investigations is, of course, very incomplete, but it is sufficient to define the regimes into which the present studies fall. These are the second and third regimes, in which the body is fairly large compared with the upstream boundary layer, and in which separation may take place at the plate leading edge. These regimes appear to be of most interest for applications such as the reduction of drag of blunt bodies or the generation of wedge-type or conical compression surfaces. Although some surface-pressure data are available for these regimes (e.g., ref. 2), no study of the flow in the separated regions has as yet been published.

The present investigation was undertaken at the NACA Lewis laboratory to provide detailed information on the flow in two typical separated-flow regions. The scope of the tests was limited to two-dimensional

bodies to permit evaluation through interferograms. The tests are preliminary in nature, and no general conclusions can be reached from the limited number of separation conditions included.

SYMBOLS

The following symbols are used in this report:

P	total pressure
p	static pressure
$\frac{\Delta p}{q_0}$	pressure coefficient, $\frac{p_1 - p_0}{\frac{1}{2}\rho_0 u^2}$
q	dynamic pressure
r	recovery factor, $\frac{T_w - t}{T_0 - t}$
T	total temperature
t	static temperature
u	free-stream velocity
θ	meridian angle of round-nose cross section measured from upstream plate
ρ	density

Subscripts:

a	free-stream stagnation
w	value at surface of model
0	free stream
1	behind shock wave

APPARATUS AND TEST PROCEDURES

All tests were conducted in the NACA Lewis 4- by 10-inch continuous-flow tunnel at a Mach number of 2.0. The tunnel was operated at two inlet-pressure - inlet-temperature combinations: 27.81 inches of mercury absolute at 62° F, and 43.36 inches of mercury absolute at 98° F. Pressure and temperature could be held within ±0.40 inch of mercury and ±2° F, respectively. The test-section Reynolds number per foot based on an inlet pressure of 27.81 inches of mercury absolute was 3.87×10^6, while that based on an inlet pressure of 43.36 inches of mercury absolute was 5.30×10^6.

Original plans were to obtain pitot-pressure, flow-direction, and density measurements for the following four models:

(1) Round-nose model (A) with separation at tip of upstream plate (fig. 1(a))

(2) Round-nose model (B) with separation on plate (fig. 1(b))

(3) Flat-faced-step model (C) with separation on plate (fig. 1(c))

(4) Flat-faced-step model (D) with separation at tip of upstream plate (not shown)

For models B and C the flow was stable, but the presence of a probe for measuring pitot pressure near the surface of the plate shifted the separation point downstream toward the body. Apparently the probe interfered with the balance between reversed flow and forward flow in such a manner that a larger pressure rise was required to separate the boundary layer. In the case of model D (plate length, 2.25 in.; step height, 0.5 in.), the flow was oscillatory, so that no data were obtainable. This instability was not unexpected and is the same as that described in detail in references 3 and 4. Pitot-probe data could therefore be obtained only for model A, but density measurements were made for models A, B, and C.

Model dimensions are given in figure 2. All models completely spanned the tunnel; a 1/4-inch band of roughness (number 80 Carborundum grit) was applied to the leading edge of each plate to ensure a turbulent boundary layer at the point of separation.

Two sets of models A and B were constructed. One of the sets, with instrumentation as shown in figures 2(a) and (b), was intended for tests giving pressure measurements, the other for obtaining interferometer data. On the former models, static-pressure orifices were placed along the centerline to provide static-pressure distributions and off center

to check two-dimensionality. Insulated thermocouples were included to give recovery-factor distributions.

Interferometer models A and B and model C were equipped with two static-pressure orifices only. These orifices were on the centerline of models A and B at distances downstream of the leading edge of 1/2 inch and $1\frac{17}{64}$ inches on model A and of 1 inch and $5\frac{15}{32}$ inches on model B. The location of the orifices on model C is shown in figure 2(c). All static pressures were read on a mercury manometer.

Pitot pressures and flow directions were measured with a cylindrical probe made of hypodermic tubing that spanned the tunnel in a direction parallel to the leading edge of the models. One end of the probe was closed and the other end was connected to a butyl-phthalate manometer. The probe was mounted so that it could be positioned at any point in the flow field over the model and could be rotated through an angle of 360°; (its opening was always over the model centerline). Tension was applied along the probe to prevent its bowing in the stream.

The effect of probe size was investigated for model A by using probes of three different diameters, 0.065, 0.040, and 0.020 inch. Results are shown in figure 3. The two larger probes produced very noticeable changes in the surface-pressure distribution. With the 0.020-inch probe, which was the smallest feasible because of breakage and time lag, the disturbances were considered sufficiently small to ensure that the probe had little effect on the flow in the separated region.

With the 0.020-inch-diameter probe, measurements were made with two different-sized orifices, 0.004-inch in diameter and 0.002-inch in diameter. No appreciable difference in pressure or flow-direction readings was found. Because the settling-out time for the probe with the smaller orifice was excessive, the 0.020-inch probe with a 0.004-inch orifice was used for all tests reported here. The probe was built up to a diameter of 0.065 inch at the tunnel walls to avoid breakage due to stress concentrations at these points. This build-up had no noticeable effect on the flow over the centerline of the model.

Flow direction at a particular location was determined by rotating the probe until a maximum pressure reading was obtained. The direction of the flow was taken as directly into the orifice, and the value of the pressure was used as the pitot pressure at the point. All the flow directions, which were taken at various points, were referenced to the free-stream flow direction (assumed parallel to the tunnel wall). The probe was calibrated by determining the flow direction at a point upstream of the separation shock.

Pressure measurements taken for the probe calibration showed that the direction of maximum pressure could be determined within ±5°. A

second peak pressure was found approximately 180° from the maximum pressure. For most points in the separated region, the magnitude of the primary maximum was much greater than that of the secondary maximum; however, for a few points both maximums had approximately the same magnitude. At one point, in fact, both maximums had exactly the same value. Points having a small difference were found to be in regions of low velocity.

Density distributions were determined by taking flow and no-flow interferograms for the models in the tunnel. A Zehnder-Mach interferometer described in reference 5 was used to take the interferograms. The light source for the interferometer was a mercury spark of 10- to 15-microseconds duration. A tunnel-inlet pressure of 43.36 inches of mercury absolute was used for the flow interferograms of models A and B, which are shown in figure 4.

A comparison of the flow and no-flow interferograms for the same model made possible the determination of density differences between points in the separated region upstream of the step. The density differences were changed to absolute densities by referencing them to a density computed at the downstream static-pressure orifice on the plate. The final densities were checked by referencing them to a point in the free stream where the density was known. For models A and B, the absolute densities calculated by the two methods agreed; however, for model C the densities based on the free-stream density were higher than those based on the density at the downstream orifice. This difference is believed to be due to a tunnel side-wall boundary-layer thickening or separation, for which no correction was possible. Because of this discrepancy, no density data are shown for model C. The agreement in densities calculated from two unrelated reference values for models A and B indicates that no significant side-wall boundary-layer correction of this data was needed. A possible reason for the greater side-wall boundary-layer effect for model C is that this model was tested at an inlet pressure of 27.81 inches of mercury absolute, whereas models A and B were tested with an inlet pressure of 43.36 inches of mercury absolute. The resulting increase in Reynolds number appears to have sufficiently thinned the side-wall boundary layer to make corrections unnecessary.

RESULTS AND DISCUSSION

Recovery Factors and Static Pressures

Recovery factors based on free-stream temperature and on local temperature are shown in figure 5 for models A and B. In both cases, the plate temperature (hence, recovery factor) in the separated region is higher than that produced by a turbulent boundary layer at the same

free-stream Mach number ($r = 0.88$). In the initial portion of the separated region, recovery factors based on local temperature (that behind the oblique shock) show lower values than would be produced by a turbulent boundary layer on a flat plate inclined at the effective separation angle.

Static pressures along the plate and over the cylindrical step are plotted in figure 6. For model A (fig. 6(a)), where separation takes place at the leading edge of the plate, a small but gradual increase in pressure occurs along the plate in the separated region. The maximum pressure is reached as the cylindrical step nears an angle θ of 45°.

The pressure attained on the plate was higher with the model used for pitot-pressure surveys than for an identical model used to obtain interferograms. For the former model, the effective wedge angle computed from the first measured pressure was 15°, corresponding to a shock angle of 45°; for the latter model, the measured shock angle was 43.5°, which corresponds to an effective wedge angle of 13.7° and a theoretical static-pressure ratio p/P_0 of 0.263. The separation process thus appears to be somewhat different for the two models, even though the models and stream conditions were as nearly identical as possible. The reason for this sensitivity is not known.

For model B, where separation occurs on the plate surface, a slight dip in pressure is noted preceding the separation (fig. 6(b)). The rapid increase in pressure near the separation point, and the plateau at a pressure about twice the upstream value are in agreement with previous results for this Mach number (ref. 2). The maximum pressure, which in this case is only a little higher than that in the plateau region, again occurs near $\theta = 45^{\circ}$ on the cylindrical nose. The data shown in figure 6(b) were obtained with the pitot-survey model (for which, however, no pitot survey could be made because of the probe effect). For this model, the pressure ratio p/P_0 in the plateau region was 0.255 which corresponds to a pressure coefficient $\Delta p/q_0$ of 0.318.

For design C (flat-faced body with separation on plate), no pitot-survey model was tested. The static-pressure orifice in the separated region for the interferometer model measured a static-pressure ratio p/P_0 of 0.259 ($\Delta p/q_0 = 0.344$), which is in agreement with the theoretical value for the measured shock angle (43.5°).

Density

Constant-density contours for the two cylindrical-nose models are shown in figure 7. In flow regions where static pressure is constant, the constant-density lines are also lines of constant total pressure

and Mach number if total temperature is assumed to be nearly constant. Such a region of constant static pressure is that above the pressure plateau on model B (fig. 6(b)) where the surface pressure is equal to the pressure behind the oblique shock. Thus, even though probe interference effects made pitot-pressure measurements impossible for this model, both Mach number and pitot pressure could be estimated from density and surface static pressures for a large part of the separated region.

A line from the beginning of separation drawn tangent to the cylindrical nose is inclined at an angle of 13.0° for model A (separation at leading edge) and 12.5° for model B (separation on plate). The effective wedge angles for these models, calculated from shock angles and surface pressures, were 13.7° and 12.5°, respectively. The tangent line from the base of the shock to the body, therefore, agrees with the effective wedge angle (perhaps by coincidence) for model B, but for model A the effective wedge angle is somewhat greater than the inclination of the tangent line. This difference may indicate that separation occurred slightly downstream of the leading edge, rather than at the edge.

The theoretical density ratio ρ/ρ_a behind the shock is 0.37 for model A and 0.365 for model B. These values are in fairly good agreement with measured values (fig. 7).

Total Pressure

Pitot-measured surveys were completed for model A only. Results are shown in figure 8 in which surface static pressures from figure 6(a) are also included. The variation of total pressure throughout the separated region is very similar to the distribution of density. In the small region of very low velocity near the cylindrical nose, the measured total pressure is slightly less than the static pressure on neighboring surfaces. It may be that this result is due to a small measuring error, but it is also possible that a centrifuging effect of the circulatory motion may be the cause.

Mach Number Distribution

For model A, Mach numbers were calculated from density and surface static pressure for the interferometer model and from total and static pressure for the pitot-survey model. For both computations, the assumption was made that, except near the cylindrical nose, static pressure is constant normal to the plate surface. Contours of constant Mach number from both of these computations are shown in figure 9(a).

Static pressures on the nose were used to extrapolate the Mach number contours to the nose surface for the pitct-survey model, but these pressures were not available for the interferometer model. For very low Mach numbers, small errors in density or static pressure produce large errors in Mach number; consequently, the precision of Mach numbers less than about 0.4 is poor.

Except in the high-Mach-number region outside, or near the edge of the mixing region, the two computed Mach numbers do not agree. This disagreement is in part related to the change in static pressure previously mentioned, and some of the difference may be due to the inaccuracy of the low Mach numbers just mentioned. However, for both models, it appears that the Mach number is less than 0.5 throughout most of the region bounded by the surfaces and a line from the shock base tangent to the body. The pitot-pressure data show stagnation at the point of highest static pressure on the model surface.

Since no pitot surveys were made for model B, Mach number could be estimated only from density and surface static pressure. For these computations, the pressures obtained with the interferometer model were used. Since only one static orifice was located in the separated region for this model, the resulting Mach numbers can be valid only over the pressure plateau region (fig. 6(b)). The resulting Mach numbers are shown in figure 9(b). The distributon is similar to that obtained with the interferometer test of model A near the outer portions of the shear region, but in the low-velocity region some differences are noted. These differences may result in part from the fact that model B has a relatively thick boundary layer upstream of separation, whereas model A has none. Model B has a correspondingly larger core of low-velocity air.

Flow-Direction Survey

Results of the flow-angle survey, made only for model A, are shown in figure 10. The arrows indicate, for the most part, the type of circulatory motion that might be expected in separated regions. The dashed line separates, with one exception, the arrows with a downstream component from those with an upstream component. The one double-headed arrow represents a point for which the pitot-pressure reading was the same in two nearly opposite directions.

Comparison of figure 10 with the Mach number distribution calculated from the pitot survey (fig. 9(a)) shows that the dividing line between upstream and downstream flow passes through the low-velocity core. Except near the plate leading edge, all Mach numbers below the dividing line are less than 0.5.

CONCLUDING REMARKS

The present study is exploratory in nature, and no general conclusions regarding velocity magnitudes or flow structure in separated regions are yet possible. The difficulties encountered in reproducing a separated flow were greater than anticipated, because the control provided by density, static pressure, and pitot-pressure measurements for the same model could not be fully used. In spite of these limitations, certain interesting results were obtained. The Mach number in the reversed-flow portion of the separated region was generally less than 0.5. For the model with separation at the leading edge of the plate, the flow-direction survey showed a reversed-flow component in about half the separated region. Surface static pressures were sensitive to the presence of probes in the separated region and to small changes in stream conditions. For this reason, detailed study of separated regions requires models that are very large relative to the minimum practical probe size. Furthermore, if several types of data are required, they should all be obtained with the same model and with exactly reproduced test conditions.

Lewis Flight Propulsion Laboratory
National Advisory Committee for Aeronautics
Cleveland, Ohio, April 11, 1955

REFERENCES

1. Kepler, C. E., and Bogdonoff, S. M.: Interaction of a Turbulent Boundary Layer with a Step at M = 3. Rep. No. 238, Dept. Aero. Eng., Princeton Univ., Sept. 1, 1953. (Contract N6-onr-270, Task Order 6, Proj. No. NR-061-049.)

2. Lange, Roy H.: Present Status of Information Relative to the Prediction of Shock-Induced Boundary-Layer Separation. NACA TN 3065, 1954.

3. Mair, W. A.: Experiments on Separation of Boundary Layers on Probes in Front of Blunt-Nosed Bodies in a Supersonic Air Stream. Phil. Mag., ser. 7, vol. 43, no. 342, July 1952, pp. 695-716.

4. Daniels, Lloyd E., and Yoshihara, Hideo: Effects of the Upstream Influence of a Shock Wave at Supersonic Speeds in the Presence of a Separated Boundary Layer. WADC Tech. Rep. No. 54-31, Wright Air Dev. Center, Wright-Patterson Air Force Base, Jan. 1954. (RDO No. 673-225.)

5. Howes, Walton L., and Buchele, Donald R.: Generalization of Gas-Flow-Interferometry Theory and Interferogram Evaluation Equations for One-Dimensional Density Fields. NACA TN 3340, 1955.

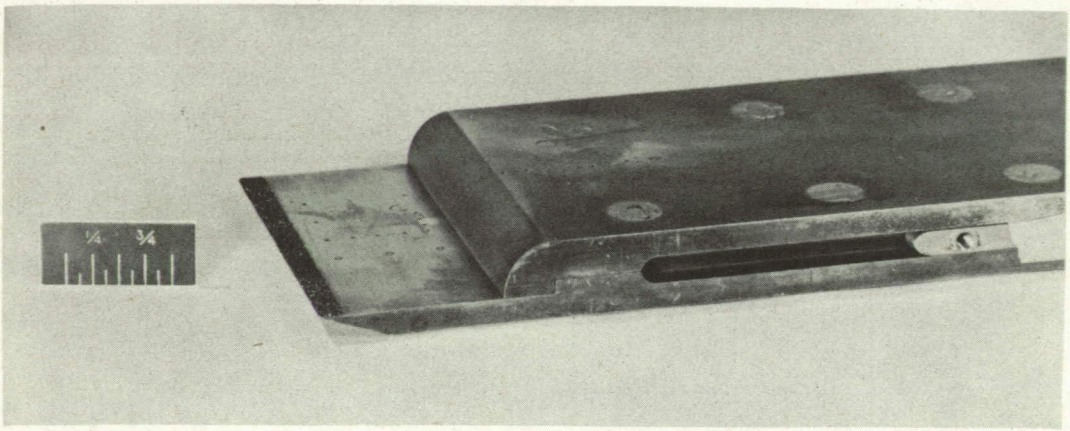

(a) Short-plate round-nose model (A).

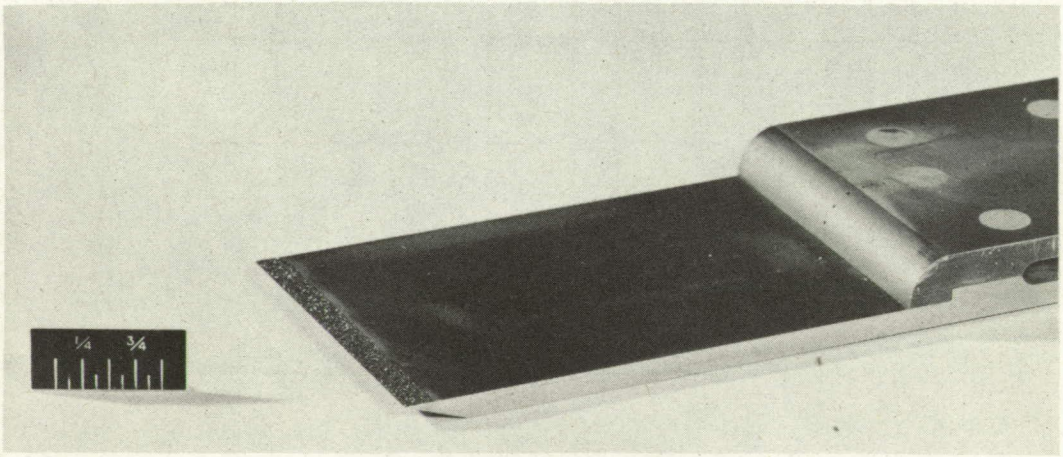

(b) Long-plate round-nose model (B).

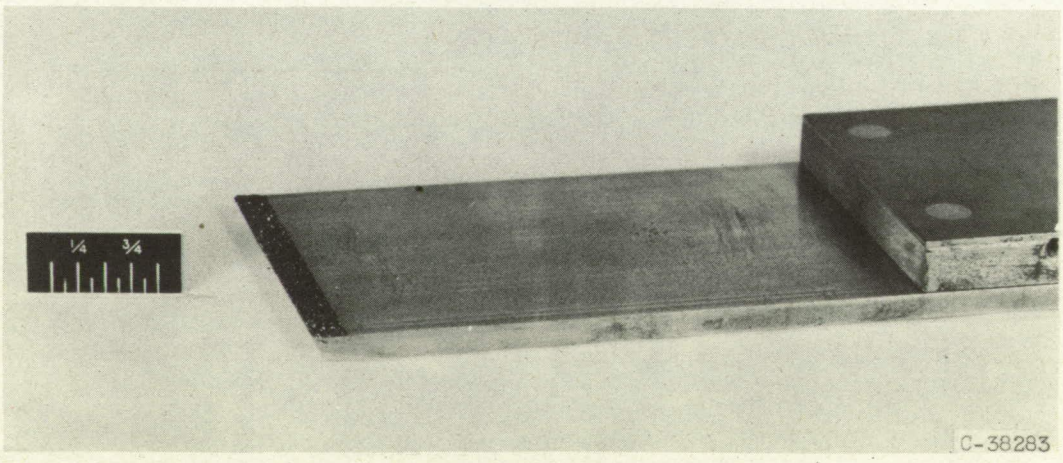

(c) Long-plate flat-faced-step model (C).

Figure 1.- Photographs of models.

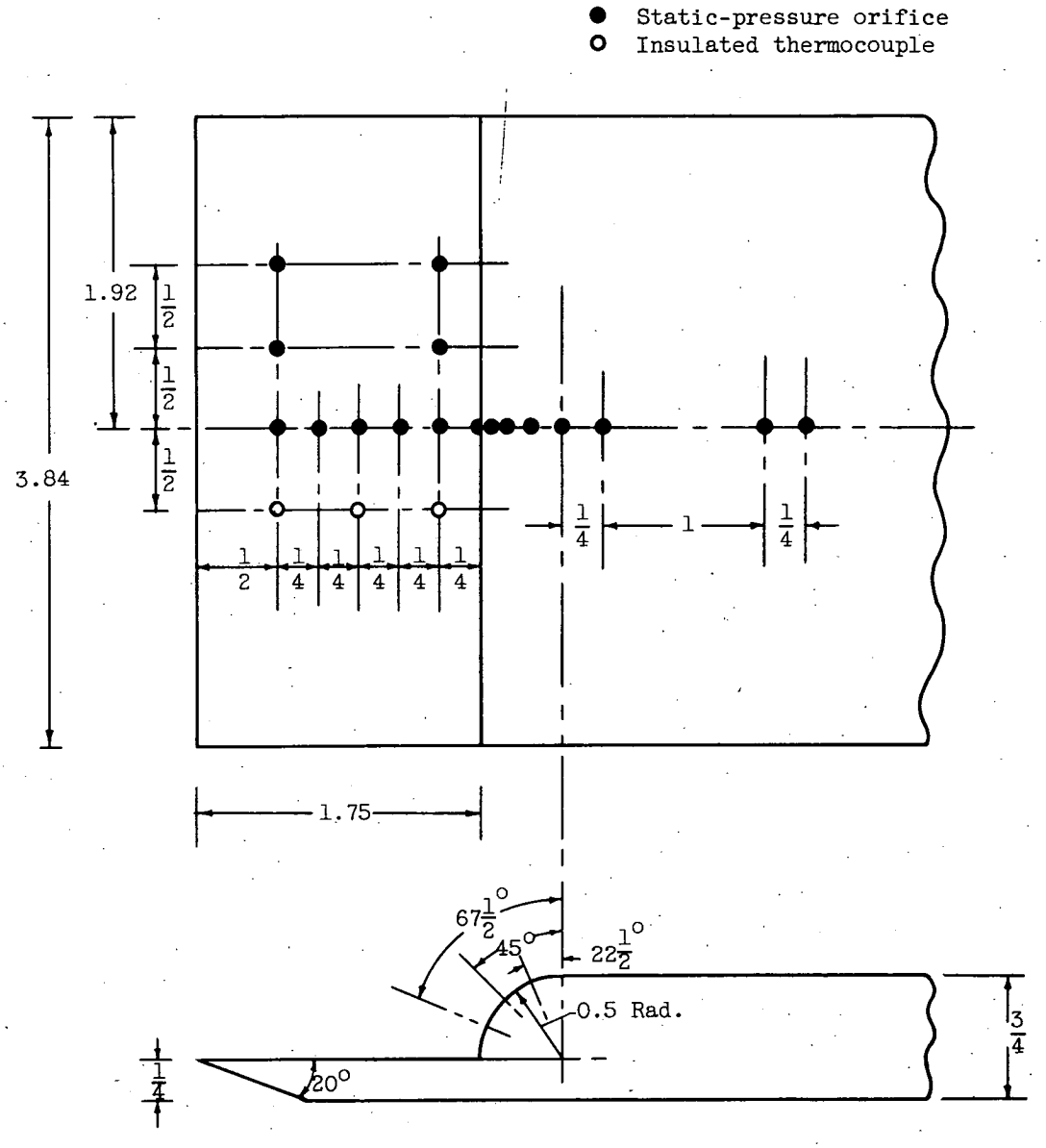

(a) Model A, for pitot-pressure measurements.

Figure 2. - Illustrations showing dimensions and location of instrumentation. (All dimensions in inches unless otherwise indicated.)

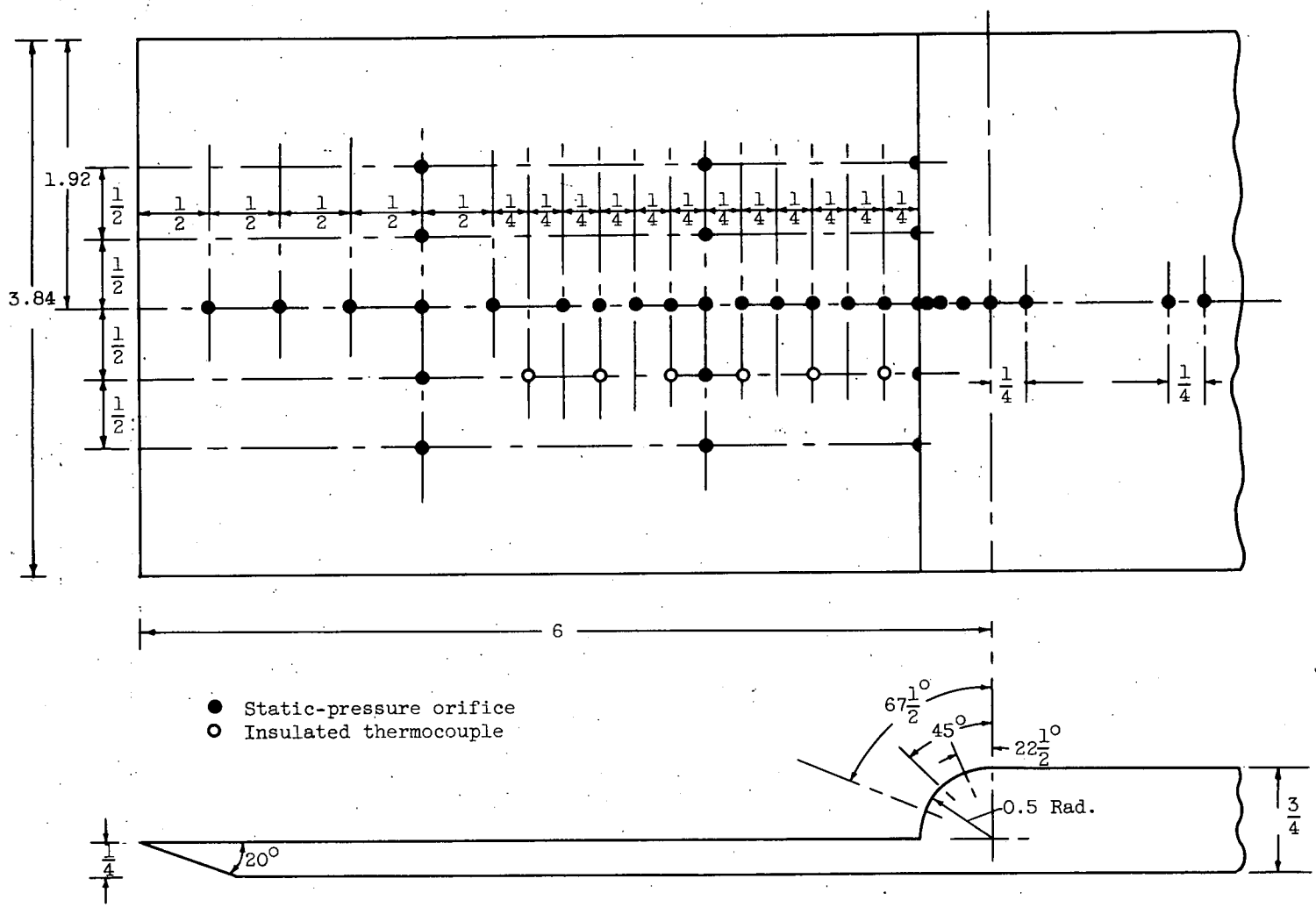

(b) Model B, for pitot-pressure measurements.

Figure 2. - Continued. Illustrations showing dimensions and location of instrumentation. (All dimensions in inches unless otherwise indicated.)

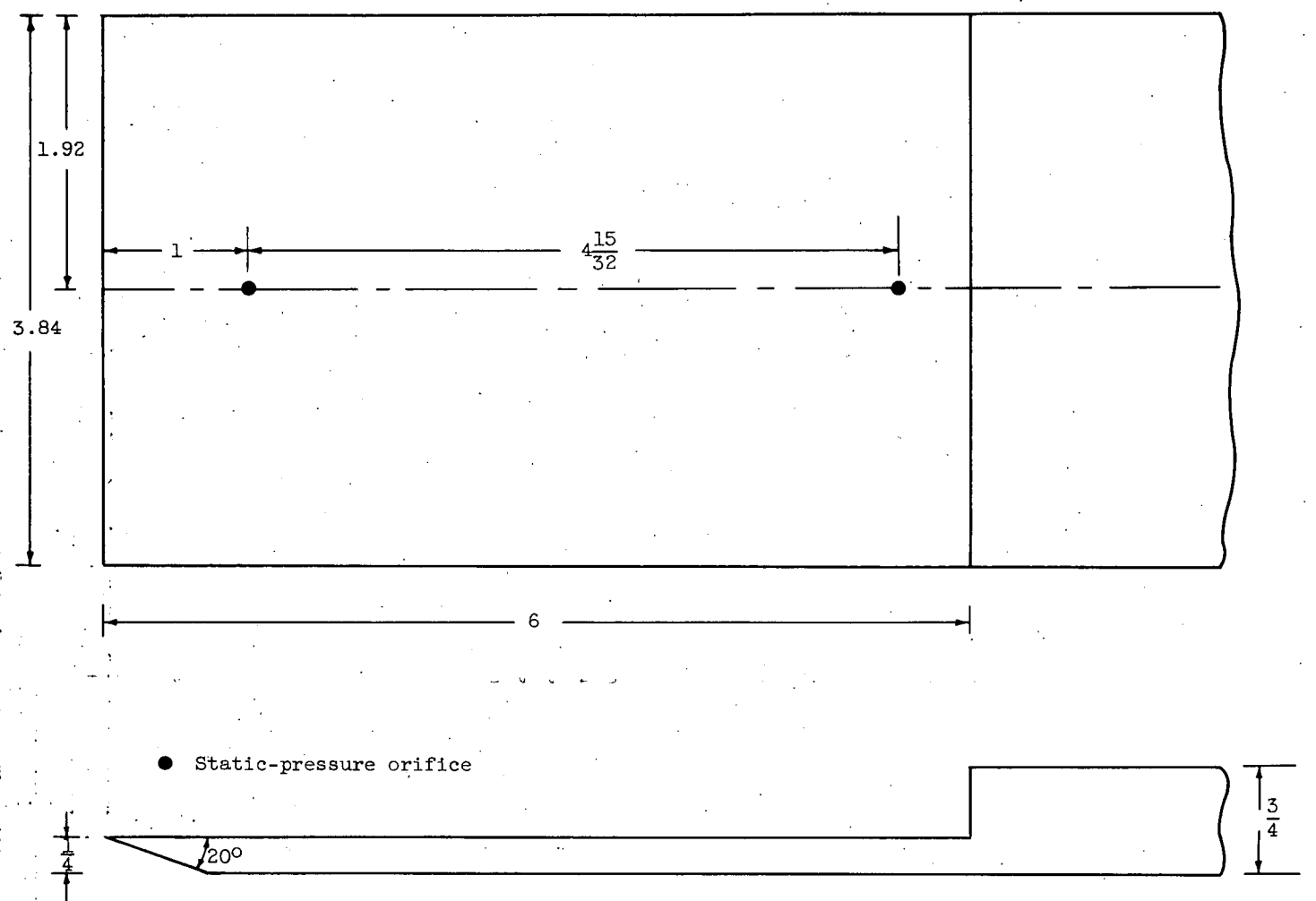

(c) Model C, for interferometer measurements.

Figure 2. - Concluded. Illustrations showing dimensions and location of instrumentation. (All dimensions in inches unless otherwise indicated.)

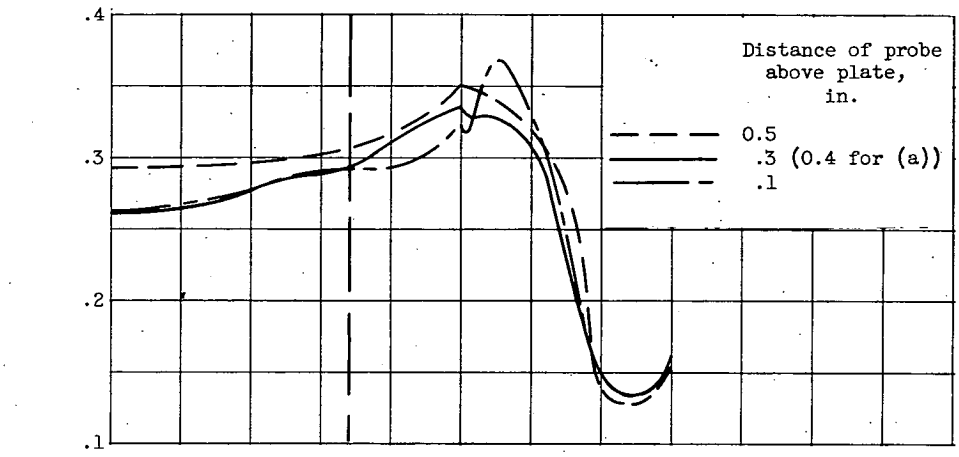

(a) 0.065-Inch-diameter probe.

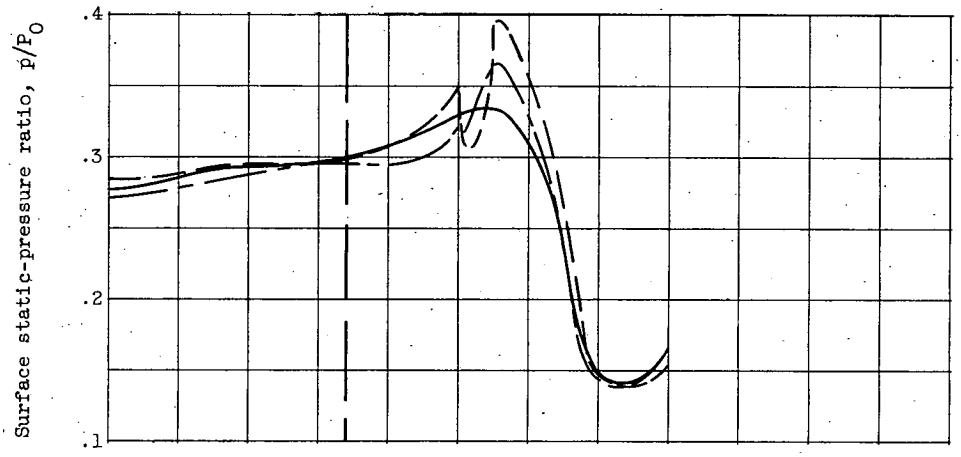

(b) 0.040-Inch-diameter probe.

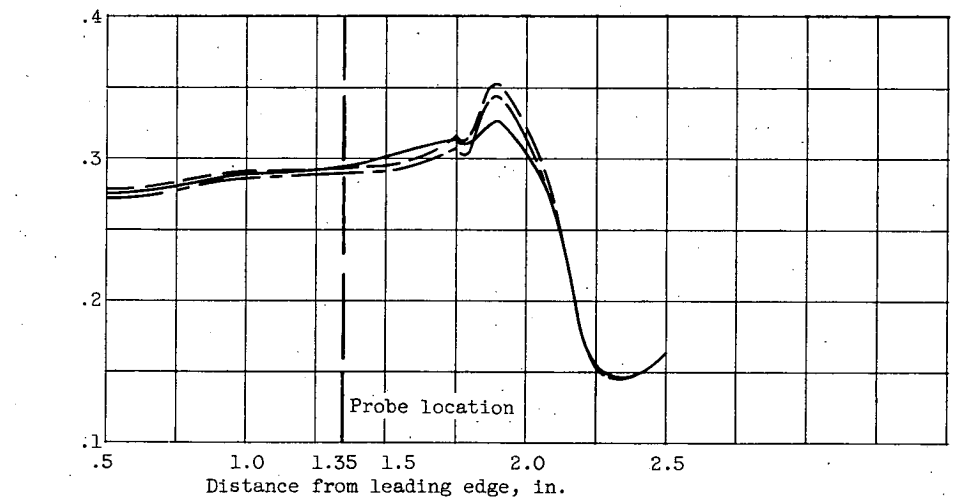

(c) 0.020-Inch-diameter probe.

Figure 3. - Influence of probe size and location on surface-pressure distribution for model A.

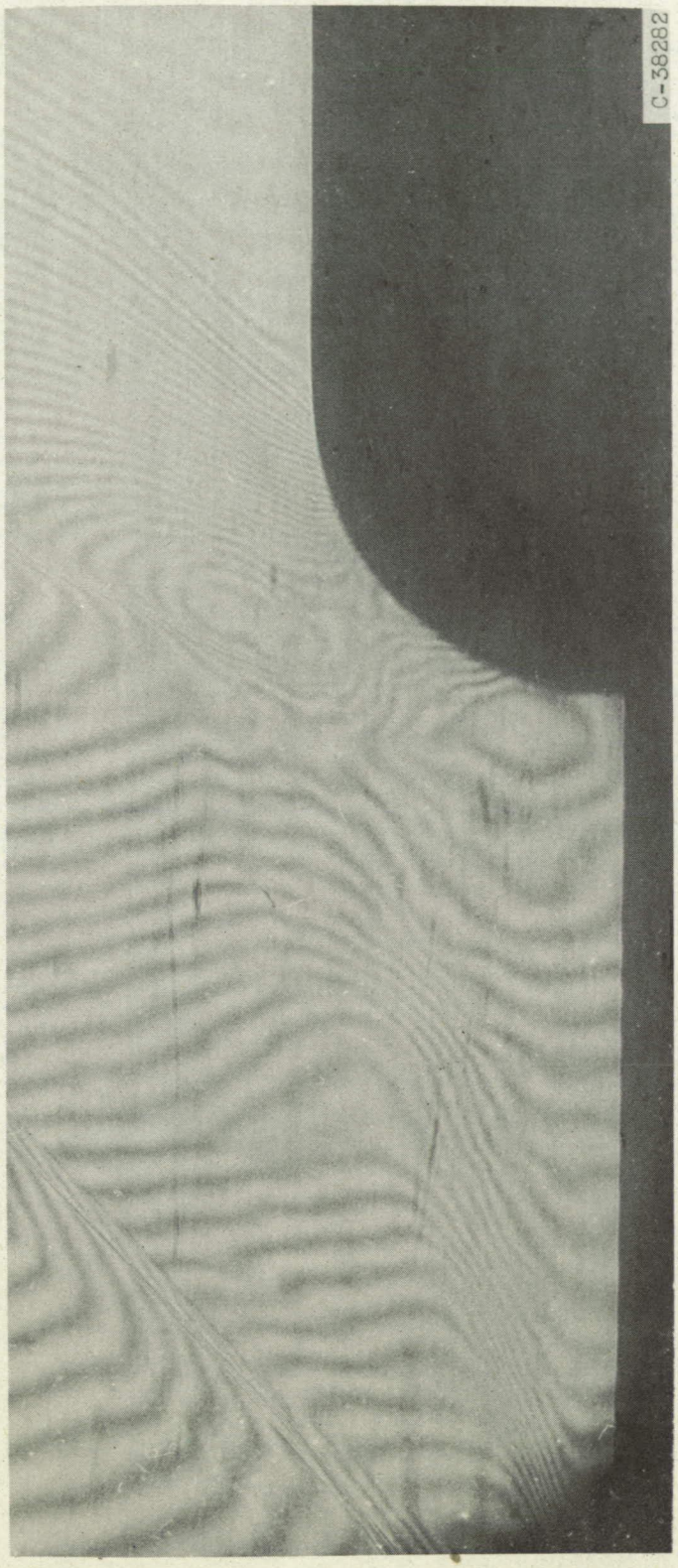

(a) Model A.

Figure 4.- Flow interferograms.

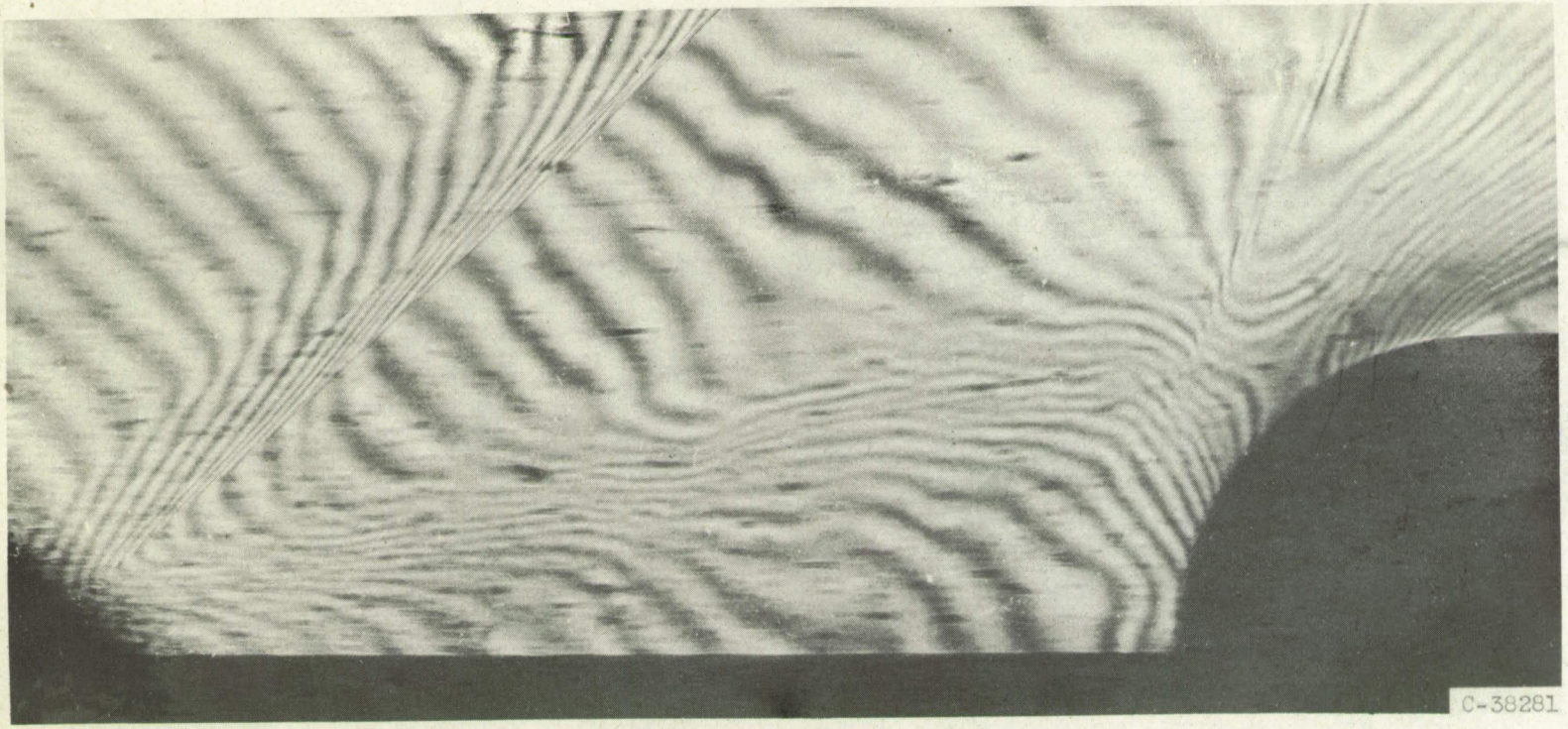

(b) Model B.

Figure 4.- Concluded. Flow interferograms.

(a) Model A.

(b) Model B.

Figure 5. - Surface-temperature recovery factors.

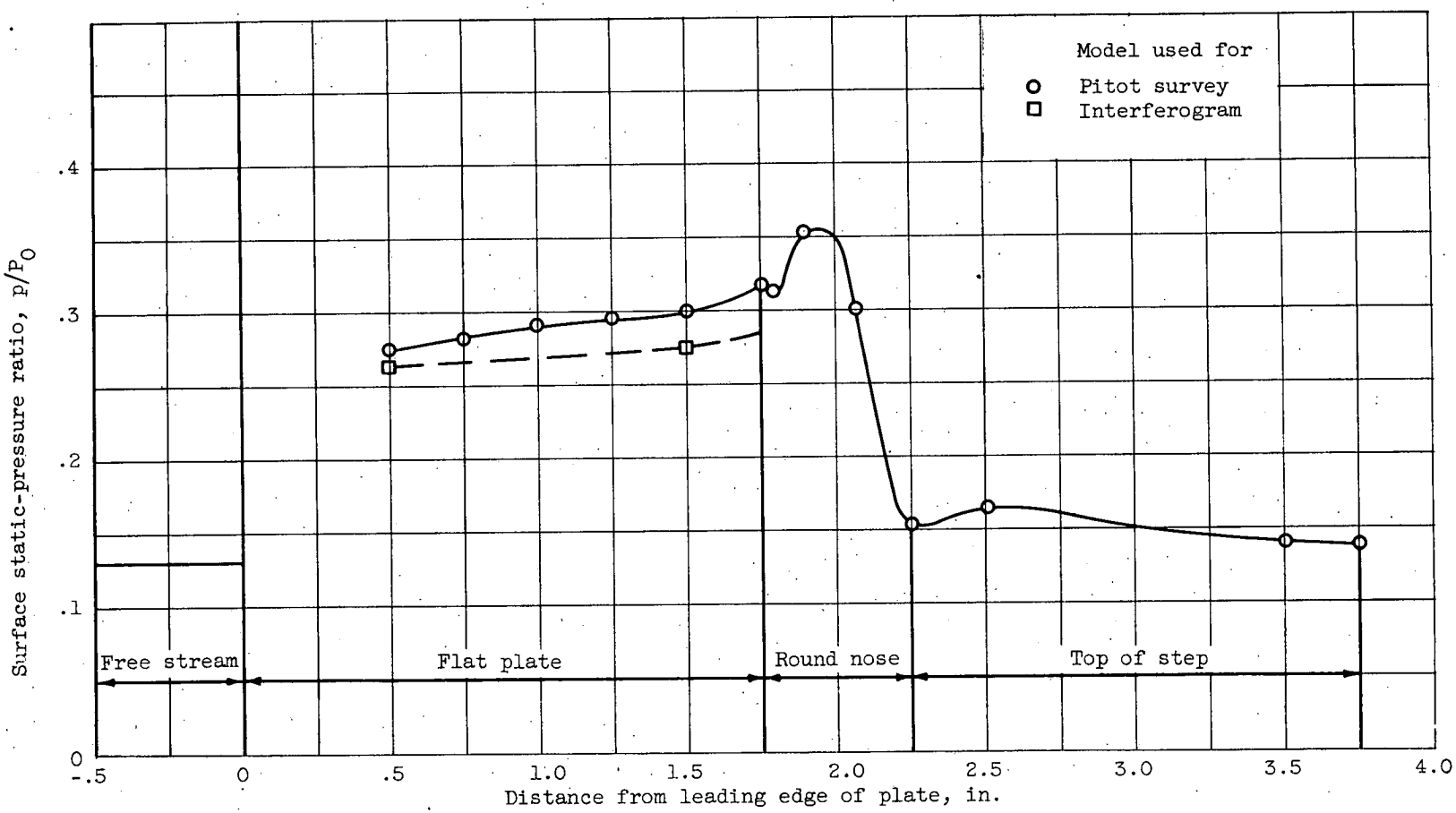

(a) Model A.

Figure 6. - Surface static-pressure distributions.

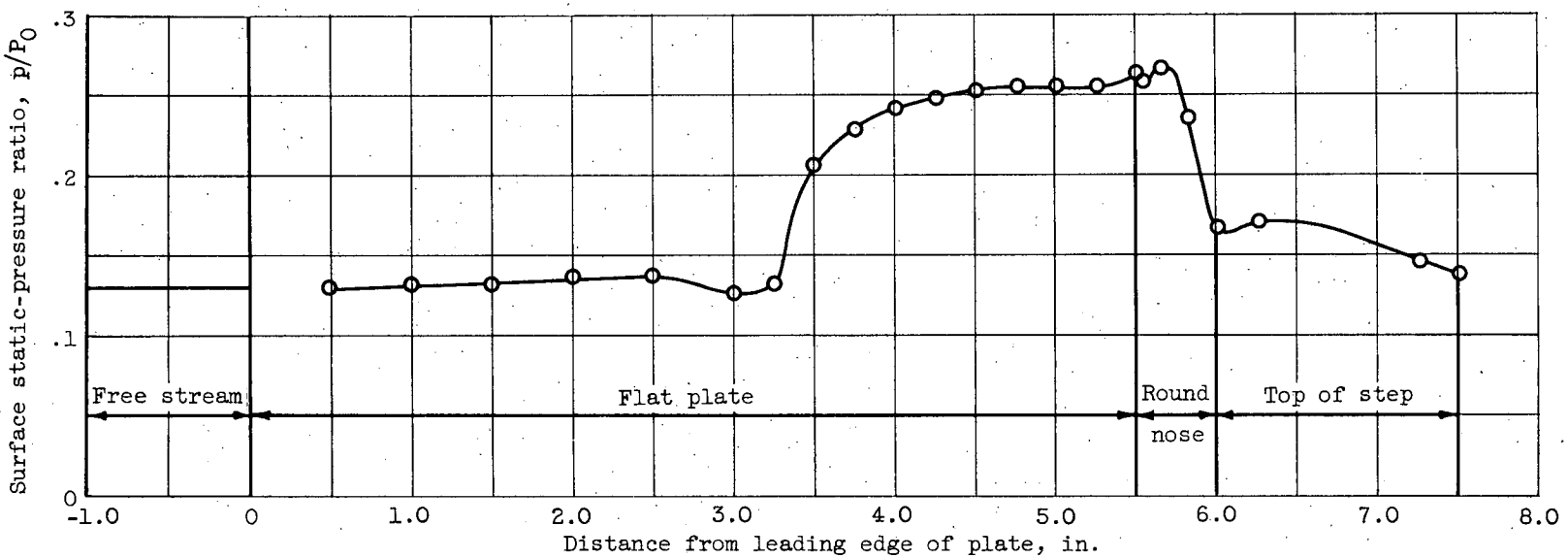

(b) Model B.

Figure 6. - Concluded. Surface static-pressure distributions.

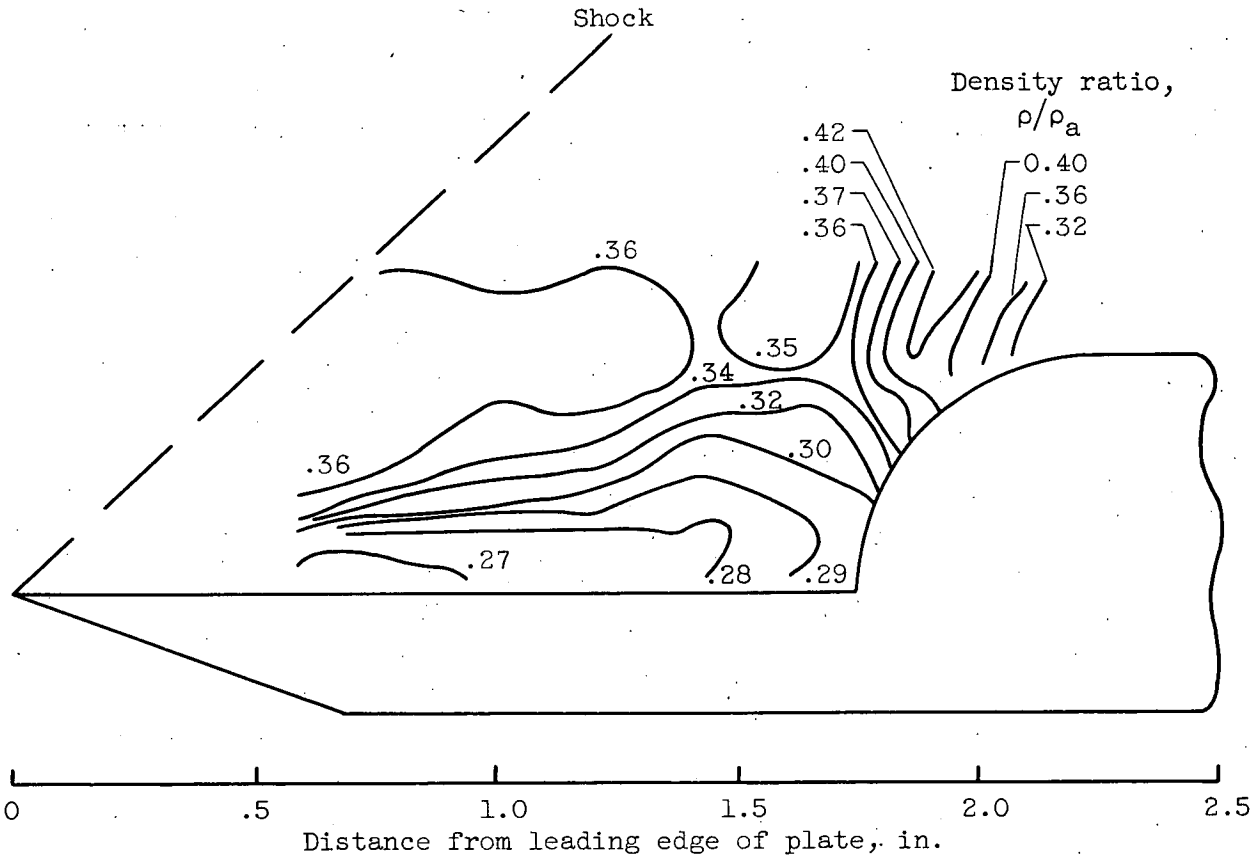

(a) Model A.

Figure 7. - Density contours.

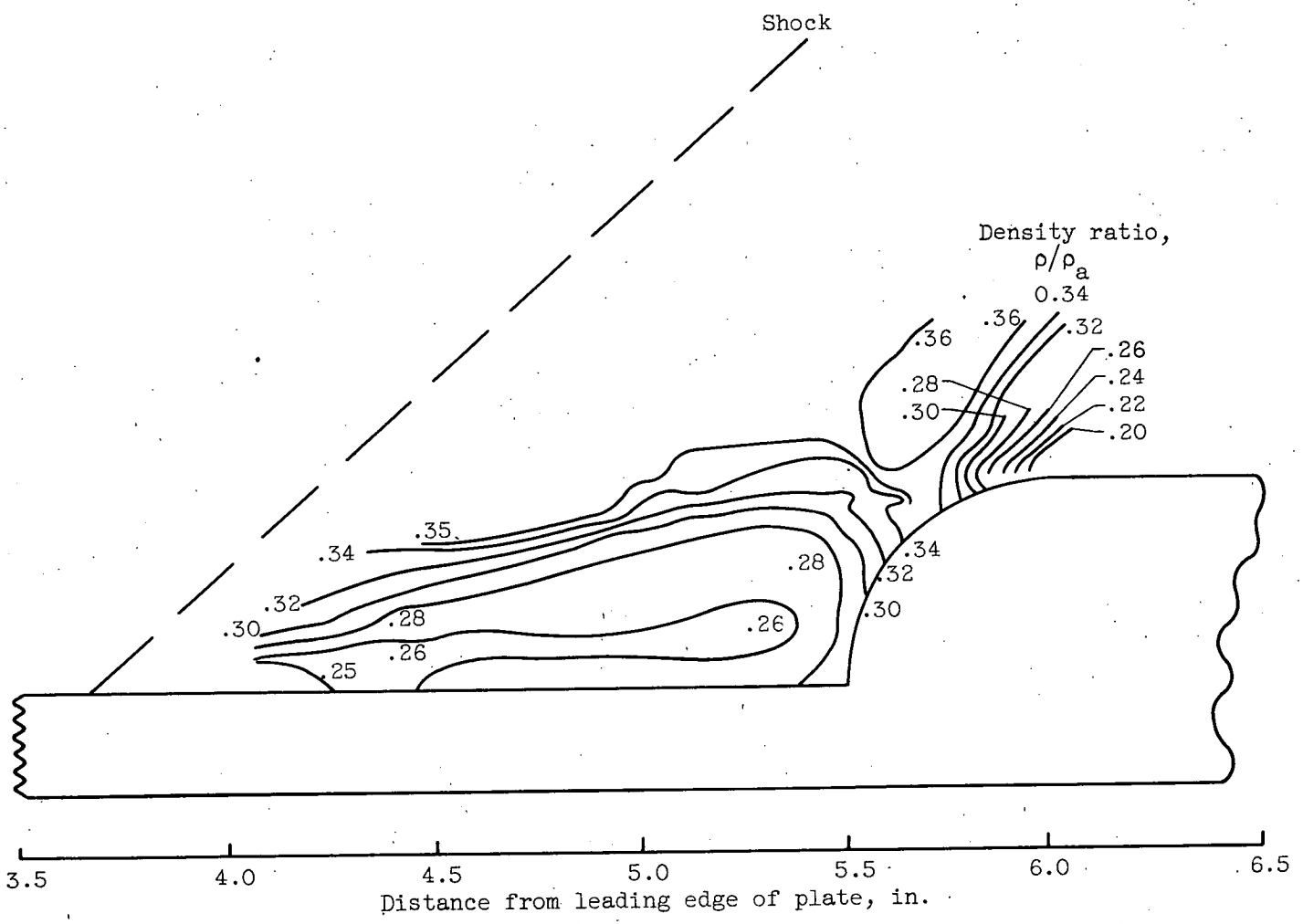

(b) Model B.

Figure 7. - Concluded. Density contours.

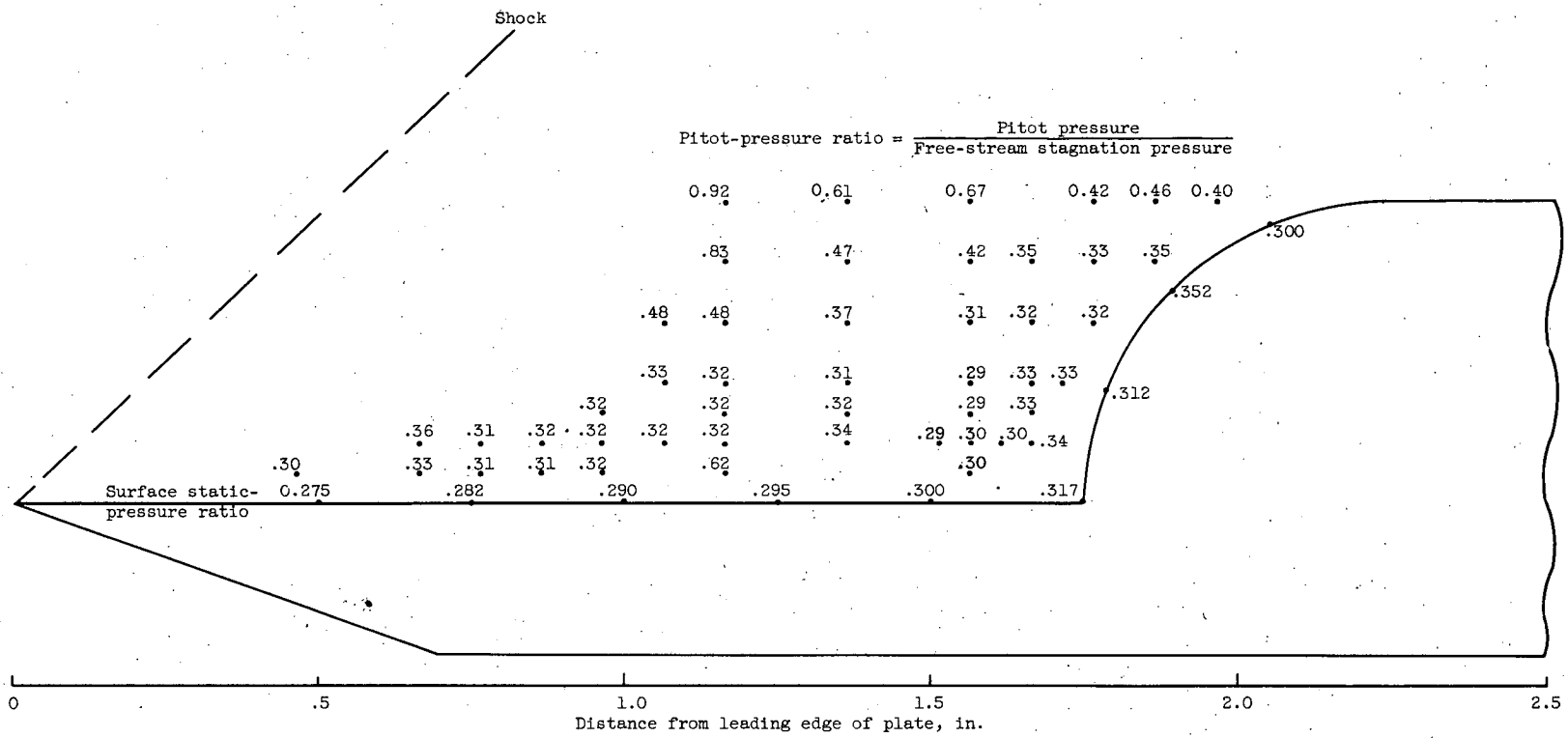

Figure 8. - Pitot-pressure distribution for model A.

Determined from pitot and static pressures

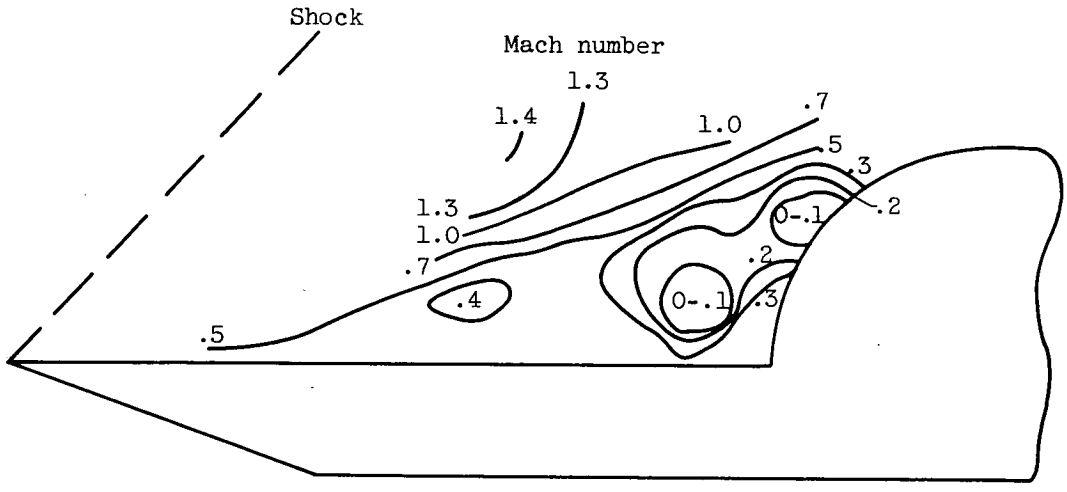

Determined from densities and static pressures

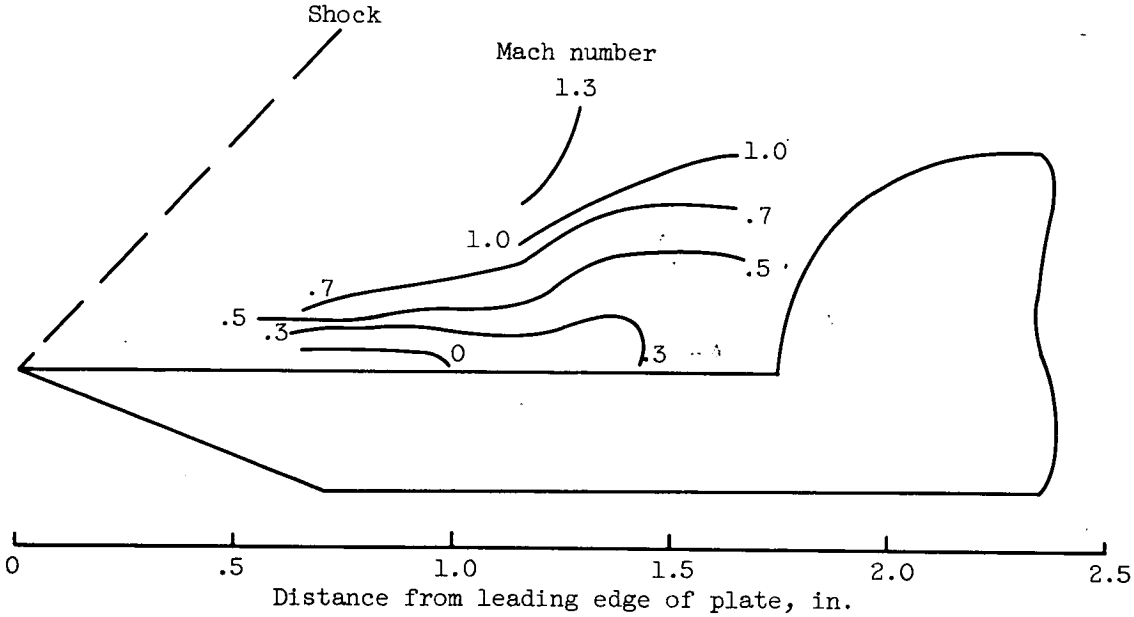

(a) Model A.

Figure 9. - Mach number distributions.

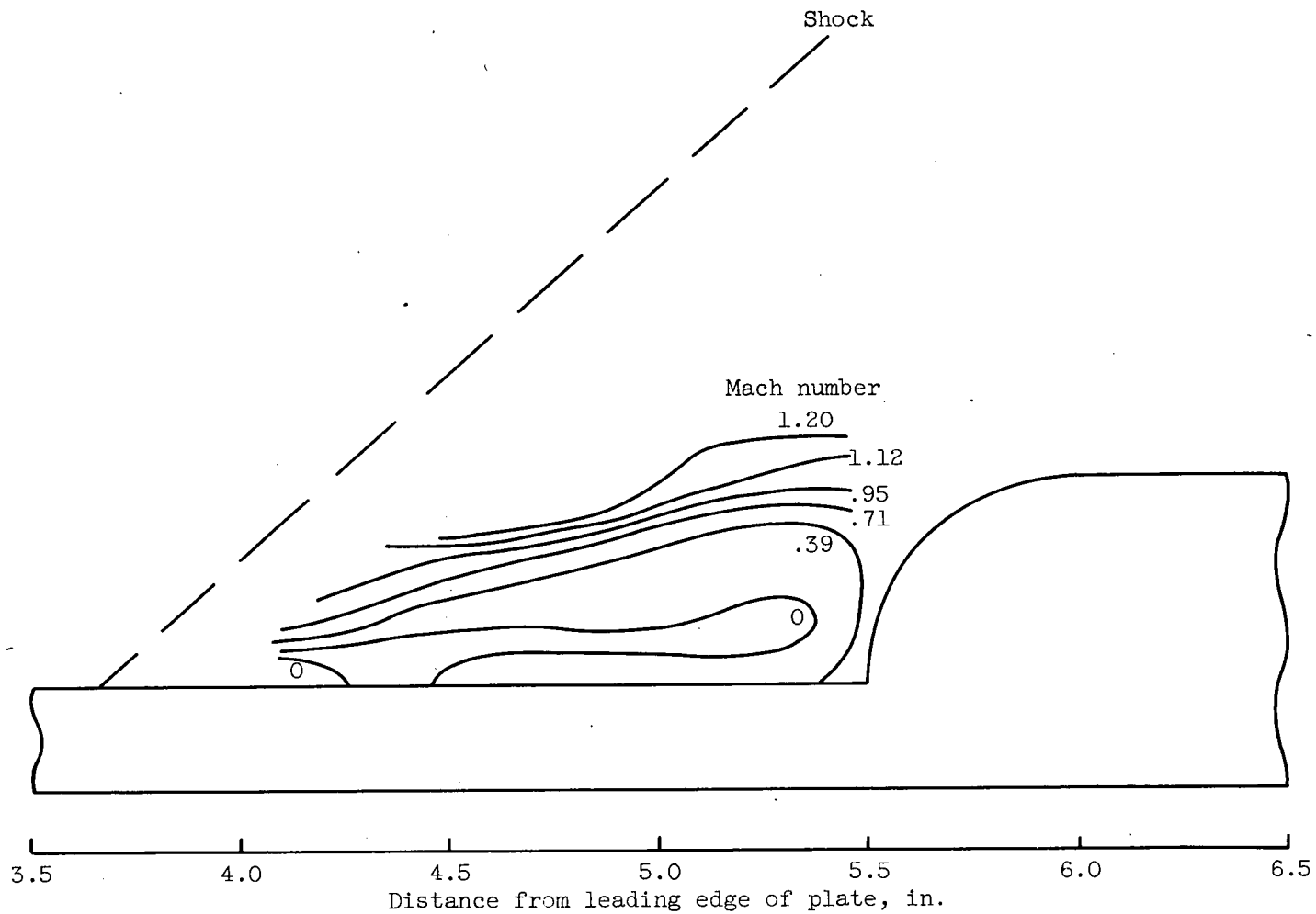

(b) Model B.

Figure 9. - Concluded. Mach number distributions.

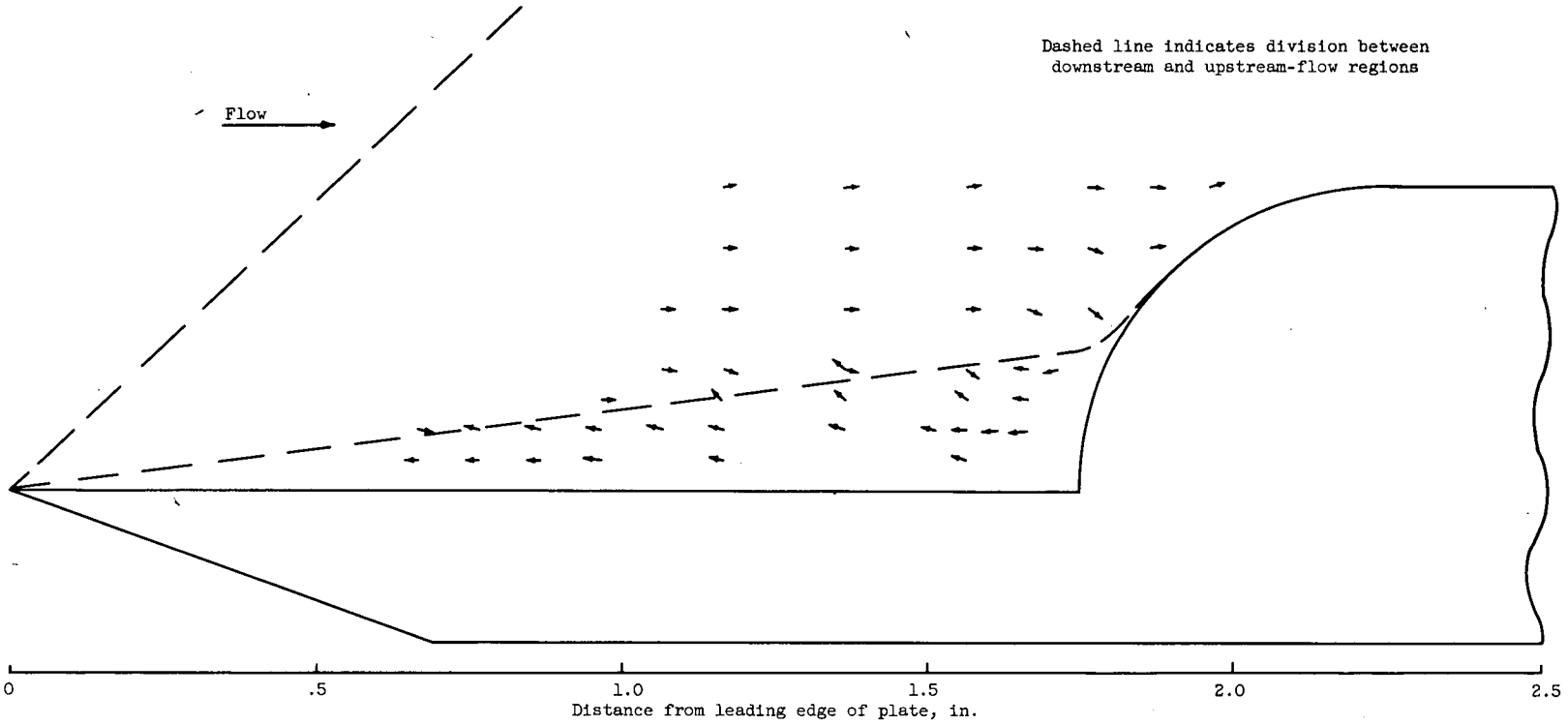

Figure 10. - Flow directions for model A.